X-621-71-242
PREPRINT

NASA TM X- 65632

A THREE DIMENSIONAL MODEL OF THERMOSPHERIC DYNAMICS

III Planetary Waves

H. VOLLAND
H. G. MAYR

JUNE 1971

GSFC — GODDARD SPACE FLIGHT CENTER
GREENBELT, MARYLAND

X-621-71-242

A THREE DIMENSIONAL MODEL OF THERMOSPHERIC DYNAMICS: III. PLANETARY WAVES

by
H. Volland
Astronomical Institutes
University of Bonn
Bonn, Germany

and

H. G. Mayr
Goddard Space Flight Center
Greenbelt, Md., USA

GODDARD SPACE FLIGHT CENTER
Greenbelt, Maryland

A THREE DIMENSIONAL MODEL OF THERMOSPHERIC DYNAMICS. III. PLANETARY WAVES

H. Volland
Astronomical Institutes
University of Bonn
Bonn, Germany

and

H. G. Mayr
Goddard Space Flight Center
Greenbelt, Md., USA

ABSTRACT

The generation and the propagation of atmospheric waves of planetary scale with zonal wave domain numbers n = 1,2,3 and 4 is calculated within the dissipative thermosphere. These waves are generated by solar XUV-heat input and by corpuscular heating of the thermosphere. They contain time independent zonal components, annual and semiannual components. The latitudinal structure of their eigenfunctions and the height variation of this structure is determined. It is shown that the relative pressure amplitudes of the wave modes approach asymptotic values at high altitudes which are proportional to $1/n(n+1)$. Therefore, the thermosphere behaves like a filter suppressing the waves with great wave domain numbers n.

The corresponding wind systems of the various wave modes are determined and compared with observed wind data at mesospheric heights as well as with density data derived from satellite drag observations. It is shown that the predominant annual component with wave number n = 1 is generated by the solar radiative heat input which peaks in the summer hemisphere and that the semiannual component containing in the mesosphere mainly the wave mode of number n = 4 is generated by corpuscular heat input within the auroral ovals.

1. INTRODUCTION

In the first part of this paper, we developed a three dimensional spherical model of the thermospherec dynamics (Volland and Mayr, 1971a; referred to as paper I). In the second part of this paper (referred to as paper II) we calculated the generation and the propagation of three important tidal waves within this model thermosphere and compared the results with available experimental data. In this third part we want to determine the wave modes of planetary scale generated by the corresponding energy modes of solar XUV and corpuscular heat inputs. These planetary waves are distinguished by their independence on local time (wave domain number m = 0). They can be divided into symmetrical terms (zonal wave domain number n is even) which describe the semiannual variations and the time independent zonal variations and into antisymmetric terms (wave domain number n is odd) which describe the annual variations. Terannual and higher order terms appear to be very weak as it follows from experimental data and theoretical considerations, therefore, we shall not treat them in this paper.

We shall calculate the equivalent depths and the eigenfunctions of the four most important planetary waves with zonal wave domain numbers n = 1,2,3 and 4. We shall determine the altitude variations in the latitudinal structure of these modes and their generation and propagation at thermospheric heights. Finally, we shall compare our theoretical result with available experimental data.

The even more important planetary wave mode of wave domain number 0, corresponding to an eigenfunction $P_0 = 1_1$ will be bypassed because this mode does not generate horizontal winds and pressure

gradients. This mode has in fact been treated in a one dimensional quasistatic model for f = 0 (Jacchia, 1965). The same wave mode with basic frequency $\omega = \Omega$ has also been considered in the Harris-Priester-model (Harris and Priester, 1962) and for various frequencies by Volland (1969) and by Thomas and Ching (1969).

2. EQUIVALENT DEPTHS AND EIGENFUNCTIONS

The determination of the equivalent depth and of the eigenfunction of the planetary wave modes follows essentially the same line as given in papers I and II. The eigenfunction describing the latitudinal structure of the relative pressure amplitude is (see (II/1))

$$\frac{p}{p_o} = \frac{p_n^f(z)}{p_o(z)} \Theta_n^f(\vartheta, z) \exp j\left(\omega t + s\Omega_a t\right) \tag{1}$$

with

$$\Theta_n^f(\vartheta, z) = \sum_{n'} \delta^f_{n,n'} P_{n'}(\cos\vartheta),$$

Using the same notation as in (II/1). Here for convenience we omitted in (1) the superscript m which is zero for the planetary waves. P_n are the zonal Legendre polynominals. The planetary waves which we shall consider and which are generated by solar XUV-heating and by the average corpuscular heat input into the thermosphere have the angular frequency $\omega = 0$ (see (I/9) and (I/12)). However, in the case of auroral heating during an individual geomagnetic storm, waves of planetary type can be generated with frequencies of the order of $\omega \sim \Omega$, where Ω is the frequency of one solar day

(Volland and Mayr, 1971b). Therefore, in order to generalize the results given below, we shall consider a frequency of

$$2f\Omega = \omega + s\Omega_a. \tag{2}$$

Apparently, it is

$$f \sim \bar{f} = \frac{\omega}{2\Omega} \quad \text{because of } \Omega_a/\Omega = 1/365,$$

where $\bar{f}$ is the Coriolis parameter introduced in (I/17).

Contrary to the general behavior of the horizontal winds of the tidal waves, the horizontal velocity of the planetary waves must be zero at the poles because the horizontal pressure gradient is zero here. Therefore, we start from the expressions for the latitudinal and the longitudinal winds of (see (II/4))

$$\frac{u}{c_o} = \Psi_n^f \frac{p_n^f}{p_o} \exp(2jf\Omega t)$$

$$\frac{v}{c_o} = \Phi_n^f \frac{p_n^f}{p_o} \exp(2jf\Omega t) \tag{3}$$

with

$$\Psi_n^f = \frac{j \sin\vartheta f_v}{2\xi\gamma} \sum_{n'} \psi^f_{n,n'-1} P_{n'-1}$$

$$\Phi_n^f = -\frac{\sin\vartheta}{2\xi\gamma} \sum_{n'} \theta^f_{n,n'} P_{n'}$$

Since the dependence on longitude of the planetary waves is zero ($\partial/\partial\lambda = 0$), the relationship between the coefficients of u and V follows from the third equation in (I/16)

$$\phi^f_{n,n'} = \frac{n'}{(2n'-1)} \psi^f_{n,n'-1} + \frac{(n'+1)}{(2n'+3)} \psi^f_{n,n'+1}. \tag{4}$$

Eq. (3) together with (4) indicate that for planetary wave modes with small frequency ω significant wind velocities can only be expected if the dissipation factors in f_v have significant magnitudes. That is certainly the case at F2-layer heights where due to ion-neutral collisions it is $|f_v| \leq 3$. However, from wind observations at mesospheric heights we have to conclude that even at those heights a dissipation mechanism must be effective (see Fig. 1).

We approximated the wind observation of fig. 1 at Adelaide (latitude: 35^o S) and in Jodrell Bank (latitude: 53^o N) by the following series of spherical functions

$$u = \sin\theta \left\{ (u_1)_o P_1 + (u_3)_o P_3 + (u_0 P_o + u_2 P_2) \cos\Omega_a t + (u_1 P_1 + u_3 P_3) \cos 2\Omega_a t \right\}$$

$$v = \sin\theta \left\{ (v_0)_o P_0 + (v_2)_o P_2 + (v_4)_o P_4 + (v_1 P_1 + v_3 P_3) \cos\Omega_a t \right. \qquad (5)$$

$$\left. + (v_0 P_0 + v_2 P_2 + v_4 P_4) \cos 2\Omega_a t \right\}$$

Where the coefficients of u and v are related with each other by Eq. (4).

Using the numbers (wind components in m/sec)

$$\begin{aligned}
(u_1)_o &= 7.5 \quad ; & (v_0)_o &= 6.2 \\
(u_3)_o &= -10. \quad ; & (v_2)_o &= 1.8 \\
u_0 &= -17. \quad ; & (v_4)_o &= -14.2 \\
u_1 &= 10. \quad ; & v_0 &= 8.3 \\
u_2 &= 22. \quad ; & v_1 &= -20.5 \qquad (6) \\
u_3 &= 25. \quad ; & v_2 &= 43.5 \\
& \quad ; & v_3 &= 33. \\
f_v &= 0.4\,j \quad ; & v_4 &= 35.7
\end{aligned}$$

we plotted our theoretical winds from (5) versus universal time t in fig. 1 as dashed lines and find satisfying agreement with the observed values appart from a prevailing wind component of the order of 10 m/sec in the wind data of Adelaine. Note that only the six coefficients u_i are available to fit the data and that $(u_1)_o$ and $(u_3)_o$ are responsible only for a shift of the vertical scale which is not very well accomplished. Considering the numbers in (6) the positive value of the imaginary part of f_v is remarkable. It can be explained readily by eddy viscosity within an atmosphere with a convex vertical profile or the longitudinal wind field. (Haurwitz, 1961). Then,

$$- \frac{\partial}{\partial z}\left(n \frac{\partial v}{\partial z}\right) \sim 2Z_{vis} \quad \Omega \rho_o v \quad \text{with} \quad Z_{vis} \sim -0.4 \qquad (7)$$

in that height range (see (I/3)). Eddy viscosity of that order and for those periods appears to be rather plausible (Kellogg, 1964). Moreover, the mean temperature profile is in fact convex between about 85 and 120 km thus suggesting a similar characteristic for the wind profile there.

This negative dissipation factor can be effective only below the turbopause at about 110 km. Above that height, ion-neutral collisions begin to dominate, thus leading to positive dissipation factors (see fig. 2)in paper II). Therefore, we may expect an effective dissipation mechanism within the lower thermosphere with a negative value below 110 km, zero at the turbopause and positive above that height.

Having tested the importance of the dissipation factors for the planetary waves, we proceed in the determination of their eigenfunctions and equivalent depths. We do this in the same manner as outlined in Paper II and look for solutions which fulfil exactly the second and third equation in (I/16) and

Eq. (II/7). Substituting Eqs. (1), (3) and (4) in the second equation of (I/16), we obtain the following relationship between the coefficients $\psi^f_{n,n'}$ and $\delta^f_{n,n'}$:

$$\frac{n'(n'-1}{(2n'-3)(2n'-1)}\ \psi^f_{n,n'-2} + \left[\frac{2n'^2+2n'-1}{(2n'-1)(2n'+3)} - f_u f_v\right]\psi^f_{n,n'} + \frac{(n'+1)(n'+2)}{(2n'+3)(2n'+5)}\ \psi^f_{n,n'+2} - (2n+1)\sum_{\nu=0}^{\infty}\ \delta^f_{n,n'+1+2\nu} = 0 \tag{8}$$

From (II/7) we obtain

$$n'(n'+1)\left\{\frac{\psi^f_{n,n'-1}}{2n'-1} - \frac{\psi^f_{n,n'+1}}{(2n'+3)}\right\} + \frac{x}{f_v f}\ \lambda_{n,n'}\ \delta^f_{n,n'} = 0 \tag{9}$$

with

$$\lambda_{n,n'}\Big\} = \begin{matrix}1 \\ 0\end{matrix} \quad \text{for} \quad \begin{matrix}n = n' \\ n \neq n'.\end{matrix}$$

An exact treatment of the eigenfunctions of planetary waves would necessitate the solution of the infinite set of the equations (8) and (9) provided $\lambda_{n,n'} = 1$ for all n' in (9). We shall do this at another place justifying there the approximate approach adopted in this paper.

The coefficients of pressure and horizontal winds in Eqs. (1) and (3) have been determined from Eqs. (8), (9) and (4) for the planetary waves with wave domain numbers n = 1, 2, 3 and 4. These coefficients can be written as

$$\delta^f_{n,n'} = \left(c_1\right)^{n'}_n / \Delta_n;\ \psi^f_{n,n'-1} = \left(c_2\right)^{n'}_n / \Delta_n;\ \phi^f_{n,n'} = \left(c_3\right)^{n'}_n / \Delta_n$$

where the numbers $\left(c_1\right)^{n'}_n$, $\left(c_2\right)^{n'}_n$, $\left(c_3\right)^{n'}_n$ and Δ_n are given in table 1. The equivalent depths become

$$h_n^f = -\frac{4 f \Omega^2 r^2 \Delta_n}{n(n+1) f_v} \tag{10}$$

According to our definition for the normalization of the eigenfunctions θ_n^f in (II/6), it is $\delta^f_{n,n} = 1$. Moreover, for large dissipation factors $|f_u|$, $|f_v| \gg 1$ it is

$$\delta^f_{n,n'} \propto 1/f_u f_v \qquad \text{for} \qquad n \neq n'$$

Thus, the eigenfunctions θ_n^f indeed approach the spherical functions P_n within the thermosphere:

$$\theta_n^0 \longrightarrow P_n \ , \tag{11}$$

and the wind functions approach

$$\begin{aligned} \Psi_n^f &\longrightarrow \frac{j}{2\gamma\xi f_u} \frac{dP_n}{d\vartheta} \ , \\ \Phi_n^f &\longrightarrow -\frac{\cos\vartheta}{2\gamma\xi f_u f_v} \frac{dP_n}{d\vartheta} \ . \end{aligned} \tag{12}$$

above about 200 km altitude. Eq. (12) shows the predominance of the latitudinal winds when compared with the longitudinal winds at thermospheric heights above 200 km where $|Z_{kin}| > 1$ which is due to the dissipation mechanisms like viscosity and ion drag.

Within the nondissipative atmosphere ($f_u = f_v = f$), the equivalent depths in (10) are negative for $f < 0.45$ to 0.7, that is, for periods exceeding about one day. The planetary waves are of the evanescent type, there. The latitudinal wind is nearly zero for small Coriolis parameters $\bar{f}$. Within the dissipative thermosphere, the waves behave like quasievanescent waves.

In the next sections we shall discuss the characteristics of the various planetary wave modes in detail.

2. PRESSURE - AND WIND FUNCTIONS

2a. Antisymmetric planetary wave modes

From the XUV-heat input distribution in (I/9) as well as from the exospheric temperature distribution in (I/14) follows the existence of the antisymmetric planetary wave mode $\theta_1^{f_1}$ $\left(f_1 = \Omega_a/2\,\Omega = 1/730\right)$ which at thermospheric heights has already degenerated to the zonal spherical function P_1. This mode describes solar XUV heat input which peaks in the summer hemisphere and it is responsible for the annual shift of the pressure bulge twoard the summer hemisphere. From fig. 1 and the numbers in Eq. (6) we have to conclude that at least within the lower thermosphere a wave mode $\theta_3^{f_1}$ exists too.

Since the frequency parameter f_1 is very small, we can set in the following $f = 0$ without significant error. Then, the wind components are exactly either in phase or in antiphase with respect to the pressure amplitude. The phase errors due to our approximation $f = 0$ are of the order of 0.5^o.

Fig. 2 gives the pressure function θ_1^0 versus co-latitude θ for the five different heights $z = 100$, 110, 150, 200 and 300 km. Here, we used the data of fig. 2 in paper II as the thermospheric parameters and approximated

$$f_u = f_v = -\,jZ_{kin} \qquad \left(Z_{kin} > 0\right).$$

However, we assumed a dissipation factor $Z_{kin} = -\,0.4$ at 100 in order to be consistent with the findings in fig. 1, and we took $f_u = f_v = 0$ at 110 km in order to simulate the situation near the turbopause. Fig. 2 indicates

the usual behavior of the eigenfunctions at thermospheric heights which we already observed in the case of the tidal waves in paper II. The eigenfunction changes from the Hough-function θ_1^0 at 110 km to the spherical function P_1 above 200 km altitude.

In fig. 3a we plotted the wind functions Ψ_1^0 and Φ_1^0 versus co-latitude for the height z = 150 km. According to table I, both wind functions do not change their latitudinal structure with altitude. Therefore we plotted in fig. 3b the maximum amplitudes of Ψ_1^0 and Φ_1^0 versus altitude. The longitudinal wind function Φ_1^0 is always negative that is, in antiphase to the pressure amplitude. However, the latitudinal wind function Ψ_1^0 is negative below the turbupause and positive (that is, in phase with the pressure) above the turbopause. At 110 km, the assumed height of the turbopause, the latitudinal wind is zero. (If we had taken into account the finite value $f = f_1 = 1/730$; the latitudinal wind function in fig. 3b would have reached a finite minimum value of 3.4×10^{-3} there.) On the other hand, the longitudinal wind function is not affected by the turbopause and reaches a maximum near 130 km altitude. Above 160 km, the latitudinal wind exceeds the longitudinal wind in magnitude.

Fig. 4a to 4c give the corresponding pressure and wind functions of the θ_3^0 - wave mode and show essentially the same features as discussed in figs. 2 and 3. The wind functions reach maximum values near 150 km. The latitudinal wind function Ψ_3^0 is zero at 110 km. It is in antiphase with the longitudinal wind above that height and in phase below that height.

It should be mentioned that our treatment of the turbulent region below the turbopause is subject to some ambiguity. We have set in the numerical

calculations of this section $f_u = f_v = 0.4j$ at 100 km altitude. However, it is by no means certain that the curvature of the height profile of the latitudinal wind is the same as that of the longitudinal wind. If the sign of f_u would be opposite to the sign of f_v, we had to expect according to table I a change of the numerical value of Δ_n toward smaller or even toward negative values. Such change can influence the amplitudes and phases of pressure and winds. This question can be resolved only by a full wave calculation eddy viscosity is inforously considered.

2b. Symmetric planetary wave modes

From the XUV-heat distribution derived in (I/9), from the distribution of corpuscular heating (I/12) and from the distribution of the exospheric temperature (I/14) we expect the existence of the symmetric planetary wave modes $\theta_2^{\,0}$ and $\theta_2^{\,f_2}$ where $f_2 = \Omega_a/\Omega = 1/365$. Both waves degenerate at thermospheric heights into the spherical function P_2. The wave mode $\theta_2^{\,0}$ describes the time independent zonal heating due to the XUV-energy input which peaks at low latitudes and due to corpuscular heating at high latitudes during equinox. The wave mode $\theta_2^{\,f}$ is responsible for the semiannual variation of these heat inputs and their corresponding density amplitudes. From (I/12) as well as from the findings in fig. 1 we expect also the wave modes $\theta_4^{\,f}$ ($f = 0$ and f_2) at thermospheric heights.

In figs. 5 and 6 we plotted in the usual way the pressure functions $\theta_n^{\,0}$ and the wind functions $\Psi_n^{\,0}$ and $\Phi_n^{\,0}$ of the two symmetric wave modes adopting again the approximation of $f_2 \sim 0$. We observe the usual behavior in amplitudes and phases of pressure and winds as discussed in section 2a.

As it is apparent from (I/9), (I/12) and (I/13), the most important symmetric planetary wave mode according to our definition is the mode with wave domain number n = 0. This mode has no latitudinal structure:

$$\Theta_0^{\,0} = P_0 = 1 ,$$

and its horizontal winds disappear:

$$\Psi_0^{\,0} = \Phi_0^{\,0} = 0 .$$

It can be treated by an one dimensional vertical model as has been done by Harris and Priester (1962), Jacchia (1965) and others.

3. WAVE GENERATION AND PROPAGATION WITHIN THE THERMOSPHERE

In order to determine the generation and propagation characteristics of the planetary wave modes at thermospheric heights, we calculated the normalized eigenvalues from Eq. (I/37) and plotted in fig. 7 the attenuation factors $\beta_n^{\,0}$ -1 versus height. They increase with increasing wave domain number n. In the case of zero frequency (f-0), all planetary waves behave like pure evanescant waves with zero propagation factor $\alpha_n^{\,0}$. In the case of the annual and semiannual wave modes ($f - f_1$ or f_2), they become quasi-evanescent with propagation factors of the order $\alpha_n^{\,0} \sim 0.01$ which is however of no relevance for their propagation characteristics.

In fig. 8 we calculated from (I/41) and (I/42) the relative amplitudes of pressure and vertical wind of the four wave modes generated at thermospheric

heights. Here, we adopted the thermospheric parameters at 300 km altitude from fig. 2 in paper II and assumed a heat input of

$$J_n^0 = \begin{cases} -0.01 & z \geq z_o \\ \text{for} & \\ 0 & z < z_o \end{cases} \qquad (13)$$

As in paper II we want to study the influence of the heat input at thermospheric heights for the generation of waves. Therefore, the lower boundary of the heat input in our model is at $z_o \sim 200$ km, and the height range $z \geq z_o$ shall simulate the situation within the thermosphere above about 200 km. The vertical dashed lines in fig. 8 give the asymptotic values of pressure and vertical winds according to Eq. (I/45). They have already been reached after 200 km in the case of wave mode θ_4^0 due to its large attenuation factor β_4^0 (see fig. 7). In the case of wave mode θ_1^0, the asymptotic values are still twice as great as the amplitudes at $z - z_o = 200$ km. True isobaric layers exist for the various wave modes between $z - z_o = 8$ km (for $n = 4$) and $z - z_o = 15$ km (for $n = 1$) where pressure and horizontal winds are zero and change their phase by 180^o. (In the case of finite frequency parameters $f = f_1$ or f_2, a finite minimum value would form there instead, and the phase transition would occur within a finite height region.) Above that isobaric layer, the pressure amplitude is greater for smaller wave domain numbers n. On the other hand, the amplitudes of vertical velocity are greater for greater n. In the case of the vertical winds, the asymptotic value is the same for all numbers n as it follows from Eqs. (I/45) and (I/47). The reason for such behavior is the following: With increasing wave domain number n, the horizontal scale length of the modes decreases. Thus, an increasing amount

of wave energy is dissipated by viscosity and ion drag which reduces the pressure amplitude. On the other hand, the number of the circulation cells increase with n (see figs. 9 and 10). In order to drive this wind circulation, the vertical velocity must be maintained. Below z_o, the height of the lower boundary of the heat input, only downgoing waves exist which decay exponentially like

$$\exp\left\{-\left(1+\beta_n^0\right)\left(z_o - z\right) / 2H_o\right\};\quad \left(z<z_o\right)$$

In fig. 9, we plotted the meridional cross-sections of the circulation cells of the antisymmetric planetary wave modes θ_1^0 and θ_3^0 corresponding to the heat input of (13) which means heat surplus on the southern hemisphere. Longitudinal winds are indicated by the symboles "W" = westerly winds (blowing from the west) and "E" = easterly winds (blowing from the east). In fig. 10 the same is plotted for the symmetric wave modes θ_2^0 and θ_4^0. Here, the heat surplus is at the equator for θ_2^0 and at middle latitudes for θ_4^0.

If we relate the wind circulations in figs. 9 and 10 to the annual and semiannual winds ($f = f_1$ or f_2), fig. 9 is valid during the December-solstice and corresponds to the heat input

$$-\left|J^0_{2n+1}\right| \cos\Omega_a t$$

Fig. 10 which gives the semiannual variation is valid during the equinox and corresponds to the heat input

$$\left|J_{2n}\right| \cos 2\Omega_a t$$

Thus, the winds in figs. 9 and 10 change direction after one half period, that is after 6 months in fig. 9 and after 3 months in fig. 10.

These circulation cells which are identical with thermally driven winds, known e. g. from the land-sea-breeze, with rising winds above the maximum heat input blowing towards the heat sink above the isobaric layer and returning below that layer should be expected throughout the thermosphere because according to figs. 3 and 6 the latitudinal winds of the various wave modes although changing their amplitudes with height do not change significantly the latitude of their phase transition. The height of the isobaric (or quasi-isobaric) layer depends on the real heat input and should lie slightly above the maximum heat input which is to be expected generally within the lower atmosphere. However, there might be an exception, namely the corpuscular heat input which terminates at the base of the thermosphere. If this heat source is able to generate a significant wave mode we would expect the isobaric layer of the corresponding wind cell near 100 km altitude. This would happen if the normalized heat input J_n^0 of the corpuscular heat source exceeds all other sources of the same wave domain number n within thermospheric heights.

It remains to discuss the implications due to the turbopause layer where a transitions occurs from eddy viscosity with negative dissipation factors into ion drag with positive dissipation factors. In order to maintain the circulation cell, we expect a wind field shown schematically in fig. 11. The latitudinal wind goes through zero at the turbopause layer without changing its phase. On the other hand, pressure and longitudinal wind change their phase abruptly although their amplitudes are not affected. In a real atmosphere such transition will of course occur within a finite height range. This behavior is quite different from the situation at the isobaric layer where pressure and both wind components become zero and change their phases as indicated in fig. 11.

4. COMPARISON BETWEEN THEORY AND EXPERIMENTAL DATA

In this section we want to compare the result of the forgoing sections with available experimental data. First, we consider the mesospheric wind data of fig. 1 and the corresponding coefficients in the series of spherical harmonics in Eq. (6). From table I and from Eq. (3), we related the observed wind components in (3) to the equivalent relative pressure amplitudes of the various wave modes. These numbers are given in table II. Considering these numbers, we have to remember our remarks in section 2a about the ambiguity concerning the vertical profile of the latitudinal wind. Therefore, the numbers in table II should be taken merely as upper limits. Especially, the annual component $\theta_1^{f_1}$ may be overestimated due to the sensitive influence of the uncertain number $\Delta_1 = 0.2 - f_u f_v \leq 0.36$ on the pressure amplitude.

Nevertheless, the numbers in table II indicate some interesting features. In the prevailing wind field (f = 0) the θ_2^0 - component predominates. The heat surplus to generate the wind cell of this mode occurs at low latitudes if we assume that the height of the mesospheric winds in fig. 1 (92 km) is below the isobaric layer of that wave mode. Then, the wind cell of this mode is that of fig. 10a. Above the isobaric layer within thermospheric heights the phase of the pressure component of this mode is consistent with the corresponding T_2^0 - term in the exospheric temperature distribution of (I/14). However the amplitude of T_2^0 in (I/14) seems to be underestimated when compared with the value suggested from table II. We can at least qualitatively explain this discrepancy by assuming that the auroral heat input terminates at about 90 to 100 km while the solar radiation reaches down to the earth's surface. Therefore the wind system due to auroral heating has its isobaric layer above 92 km

while the wind system due to XUV heat input has its isobaric layer far below that height. Thus in the height range around 90 km both contributions to the horizontal wind and pressure fields add together, whereas at thermospheric heights they compensate each other due to the reversed signs in the corresponding heating terms in (I/9) and (I/12).

The wind direction of the longitudinal wind component at thermospheric heights of the Θ_2^0 -mode is consistent with the westerly prevailing winds discovered by King-Hele (e.g., King-Hele and Allan, 1966). However the amplitude of this wind component estimated from the number in (I/14) and from figs. 5c and 8 is

$$\left|(v)_2^0\right| \sim 5 \text{ m/sec}$$

at 200 km altitude and is one order of magnitude smaller than King-Hele's wind. Moreover, the longitudinal wind of the Θ_2^0 - mode disappears at the equator which seems to be inconsistent with the findings of King-Hele. Therefore, King-Hele's prevailing winds can not be explained by the zonal Θ_2^0 -mode.

Even if we assume that Jacchia's (1965) temperature component $T_2^0 = -7^o$ K in (I/14) is an underestimate and that the full contribution of the XUV - heat input in (I/9) is effective (neglecting the corresponding component of the corpuscular heat input in (I/12)) we arrive at an upper limit of the temperature amplitude of the zonal (2,0) mode of

$$\left|T_2^0\right| \lesssim 13^o \text{ K}$$

as compared with $\left|T_1^{1,1/2}\right| \sim 120^o$ K of the fundamental diurnal mode.

That relatively small component of the zonal (2, 0) mode is the result of the filtering effect of the thermospheric dynamic system which suppresses higher order components of pressure and temperature like 1/n(n+1) (see (I/47) and (I/49)). This is the explanation for the small observed zonal temperature amplitude in (I/14).

The $\theta_4^{\,0}$ -wave mode can be explained as generated by the corresponding corpuscular heat input term in (I/12) if the isobaric layer of the wind cell is above 92 km, the height of the observed winds in fig. 1. Then, the wind cell of this mode has the form of fig. 10b however with reversed wind directions with westerly winds at low latitudes above the isobaric layer. These longitudinal winds may be added to the winds of the $\theta_2^{\,0}$ -mode. However, at high latitudes the winds of this mode are easterly. The maximum westerly wind of the $\theta_4^{\,0}$ -mode at 200 km altitude is estimated from (I/12) and figs. 6c and 8 as

$$\left|(v)_4^{\,0}\right| \leq 1 \text{ m/sec}$$

which again is too small to explain the King-Hele-wind. The relative pressure amplitude of this mode at thermospheric heights is expected from the corpuscular heat input in (I/12) and already transformed into Jacchia's (1965) exospheric temperature amplitude is

$$\left|T_4^{\,0}\right| \leq 2^{o}\,K \qquad (T_o = 1000^{o}\,K)$$

which appears to be not very significant.

We now turn to the annual components in table II. Here, the $\theta_1^{\,f_1}$ - component predominates although the number in table II may be overestimated as already mentioned. This component is consistent with the corresponding

XUV-heat input term in (I/9) and with the exospheric temperature term in (I/14) if the isobaric layer of this mode is well below 92 km, the height of the wind in fig. 1. Then, the heat surplus occurs on the summer hemisphere and can readily be explained as resulting from the solar radiative heat input which peaks in the summer hemisphere during solstice.

From (I/9) and from the result of section 3 we estimate a pressure component related to the pressure of the fundamental symmetric diurnal mode $\theta_1^{1,1/2}$ (see paper II, section 3) of

$$\left|\frac{p_1^{f_1}}{p_1^{1,1/2}}\right| \sim \left|\frac{J_1^{f_1}}{J_1^{1,1/2}}\right| = 0.4$$

which agrees completely in amplitude and phase with the corresponding number of the exospheric temperature distribution of (I/14):*)

$$\left|\frac{T_1^{f_1}}{T_1^{1,1/2}}\right| \sim \frac{0.048}{0.12} = 0.4$$

---

*) Note that Jacchia's exospheric temperature (Jacchia 1965) represents merely the density amplitude above about 200 km. A ratio of $T_n^m/T_o = 0.1$ corresponds to a relative density amplitude of $\rho_n^m/\rho_o \sim 0.4$ for $T_o = 1000^o$ K and above 200 km. Moreover, the density amplitude is proportional to the pressure amplitude, and it is $\rho_n^m/\rho_o \sim 0.85 p_n^m/p_o$ within thermospheric heights above about 200 km.

The wind cell of fig. 9a is just the wind circulation proposed by Kellog (1961) and by Johnson (1964) to explain the F2-layer winter anomaly and the winter helium bulge. Moreover, from our result in section 2, from fig. 11 and from (I/42) it follows that within the turbulent region with convex wind and temperature profiles the pressure and temperature are out of phase with the latitudinal wind. Therefore, in the height region near 90 km we expect a cold summer pole and a warm winter pole which is consistent with experimental data (Cole and Kantor, 1963). The amplitude of this observed temperature wave is of the order of $T_1^{f_1}/T_o \sim 0.25$ at 90 km altitude which is quite consistent with the number given in table II.

We estimate the maxima latitudinal wind at 200 km from the number in (I/9) and from figs. 3b and 8 as

$$\left|(u)_1^{f_1}\right| \sim 25 \text{ m/sec}$$

which is a reasonable value to explain the F2-winter anomaly.

The $\theta_3^{f_1}$ -component in table II has the opposite sign of the $\theta_1^{f_1}$-component. Therefore provided the heat input maximum occurs below 90 km, its corresponding wind cell has the form of fig. 9b, however, with opposite wind direction. That is equivalent to a heat surplus on the winter pole. The corresponding XUV-heat input term is very small (in our approximation in (I/9) it is exactly zero). The origin of this component seems to be obscure, therefore. It may perhaps be related to the real heat distribution within the lower atmosphere where such term would damp the pure $\cos\theta$ - dependence of the annual heat variation as the result of some horizontal heat transfer from the summer to the winter hemisphere.

Next, we consider the semiannual components in table II. The latitudinaly depending part of the semiannual effect at thermospheric heights is according to table II predominantly included in the $\theta_4^{f_2}$ -mode. Its phase in table II is consistent with the corresponding corpuscular heating term in (I/12) if we assume that the isobaric layer of that mode is above 92 km, the heights of the winds fig. 1. This behavior, therefore, can be considered as typical for wind systems driven by the corpuscular heat input. The wind system of this mode is that of fig. 10b, however, with reversed wind direction.

We estimate from the number in (I/12) and from the results of the foregoing sections a pressure amplitude of this mode above 200 km already transformed into the exospheric temperature amplitude of

$$\left|\frac{T_4^{f_2}}{T_o}\right| \leq 0.0005$$

which is completely insignificant at thermospheric heights.

The small $\theta_2^{f_2}$ component at 92 km (see table II) does not fit into the general picture outlined above because it should be relatively large as compared with the $\theta_4^{f_2}$ component due to the additive effects of solar radiation and auroral heating at this height range (see the remarks in connection with the zonal θ_2^{0} component). However at thermospheric heights we expect rather small amplitudes of the $\theta_2^{f_2}$ component with an upper limit of the temperature amplitude according to (I/9) of

$$\left|T_2^{f_2}\right| \leq 3^{o}\ K \qquad (T_o = 1000^{o}\ K),$$

which is not inconsistant with Jacchia's analysis in (I/9).

Finally, we want to estimate the amplitudes of the zonal and the semi-annual (0, 0) modes generated by solar XUV and auroral heating. We do this by adopting the half empirical formula (I/49) which is valid for n = 0 and which gives rather good approximated values at thermospheric heights as has been tested by full wave calculations. Since the fundamental diurnal mode $\Theta_1^{1,1/2}$ has the well established temperature amplitude of $\left|T_1^{1,1/2}\right| \sim 120^{o}$ K during moderate solar activity ($T_o = 1000^{o}$ K) we shall use this value as a normalizing factor. A second normalizing factor will be adopted from the upper limit of the corpuscular heat input in (I/15). Then we determine from (I/9), (I/12), (I/15) and (I/49) a zero component of the exospheric temperature of

$$T_0^{\,0} \leq \frac{2.4 \times 1.17 \times 120}{0.4 \times 1.83} = 460^{o}\ \text{K} \qquad (14)$$

as the mean temperature at thermospheric heights due to the contributions of solar XUV and auroral heating. This temperature amplitude is smaller by a factor of about two when compared with the observed mean exospheric temperature of $T_o = 1000^{o}$ K in (I/14). The number in (14) is quite consistent with the finding of Jacchia (1965) that the observed mean exospheric temperature extra - polated to zero solar activity is about 500^{o} K.

We therefore need an additional heat source to generate the residual 500^{o} K temperature. Several heat sources have been proposed. Hines (1965) assumed heating due to wave dissipation of the whole spectrum of gravity waves within thermospheric heights. Volland (1969) assumed wave dissipation of the fundamental diurnal mode. Lindzen and Blake (1970) proposed wave dissipation of the semidiurnal modes. Since the semidiurnal waves are propagation modes within the lower atmosphere with relatively large amplitudes near 100 km height, Lindzen and Blake's (1970) assumption is probably the most likely one.

The mean heat input due to that dissipated energy in (I/13) has the amplitude

$$Q^{o}_{dis} \geq 1.4\, Q^{o}_{XUV} \tag{15}$$

during moderate solar activity ($T_o = 1000^o$ K).

Turning to the semiannually varrying (0, 0) component in (I/12) we arrive at an amplitude of the corpuscular heat input of

$$\left| T_0^{f_2} \right| \leq 13^o \text{ K.} \tag{16}$$

From Jacchia's analysis (I/14) we find an amplitude of

$$\left| T_0^{f_2} \right| = 40^o . \tag{17}$$

Therefore an additional heat source must be effective to generate the temperature difference which is again most likely due to wave energy dissipation of tidal waves (Volland, 1969). We estimate its energy amplitude from the numbers in (14) to (17) using the already mentioned assumptions as

$$\left| Q_0^{f} \right|_{diss} \sim -0.05\, Q^{o}_{dis}$$

which is just the value proposed in (I/13).

5. CONCLUSION

We considered in this paper planetary waves at thermospherics heights generated by solar XUV-heat input and by corpuscular heating. We determined the eigenfunctions of the four most important planetary waves with zonal wave domain numbers n = 1,2,3 and 4 and showed the height dependence of the latitudinal structure of these eigenfunctions. Due to dissipation forces like

viscosity anol ion drag, the eigenfunctions of the wave modes become essencially identical with the zonal spherical harmonics $P_n(\cos\theta)$ above about 200 km.

We calculated the generation and the propagation of the various wave modes within the dissipative thermosphere. It has been shown that the relative pressure amplitudes and the horizontal winds of the wave modes approach asymptotic values at high altitudes which are proportional to (1/n(n+1). Therefore, the thermosphere behaves like a filter for the pressure amplitudes and the horizontal winds suppressing waves with large zonal wave domain numbers n. However, the amplitudes of the vertical winds have the same asymptotic value for all wave modes.

The corresponding wind systems of the various wave modes have been determined and compared with observed wind data at mesospheric heights as well as with density data derived from satellite drag observations. The following conclusions have been drawn:

1. The prevailing winds (zero period) containing the components n = 2 and 4 are rather strong at mesospheric heights, however small at thermospheric heights. The Θ_2^0 -component has its origin in solar radiation and in auroral heating. Both heating components which are in antiphase contribute additionally to the winds and pressure fields near 90 km because the auroral heat input which terminates near 100 km altitude generates a wind cell with an isobaric layer above 90 km. On the other hand, the solar radiation generates a wind cell with an isobaric layer below that height. At thermospheric heights, however, the winds and pressure fields of both heat

sources compensate each other. The θ_4^0 -component can be explained as generated mainly by auroral heating.

2. The annual winds with components n = 1 and 3 are strong at mesospheric heights. The $\theta_1^{f_1}$ -component is also significant at thermospheric heights and can be explained by the solar radiative heat input which peaks in the summer hemisphere during solstice. Due to eddy heat conductivity at mesospheric heights below the turbopause, a cold summer pole near 90 km altitude is expected from our theory which is consistent with observations (Cole and Kantor, 1963). The $\theta_3^{f_1}$ -component is strong at 90 km, however supressed already at thermospheric heights due to the filtering effect of the thermosphere. Its origin is obscure.

3. The semiannual wind component $\theta_2^{f_2}$ is insignificant at 90 km as well as at thermospheric heights. This is explained by the compensating effect in the corresponding components of XUV and corpuscular heating. The $\theta_4^{f_2}$ -component predominates the latitudinal structure of the mesospheric winds near 90 km. It is explained as originating from the corresponding heating term in the auroral heat input.

4. The mean exospheric temperature can be considered as the temperature amplitude of the zonal wave mode with wave domain number n = 0 and zero frequency (f = 0). It is generated by solar XUV heat input and to a significant amount by the dissipated wave energy due to tidal waves from the lower atmosphere. The semiannually varrying zonal wave mode $\theta_0^{f_2}$ has its origin mainly within the lower atmosphere and results from wave dissipation of planetary waves from below.

6. Literature

Cole, A. E. and A. J. Kantor — 1963 — Air Force interim supplemental Atmosphere to 90 km. Air Force Surveys in Geophysics No. 153, 29 pp. AFCRL-63-936, Air Force Cambridge Research Lab., Bedford, Mas.,

Harris, I. and W. Priester — 1962 — Time dependent structure of the upper atmosphere. Journ. Atm. Sci. 19, 286-301

Haurwitz, B. — 1961 — Frictinal effects and the meridional circulation in the mesosphere. Journ. Geophys. Res., 66, 2381-2391

Hines, C. O. — 1965 — Dynamic heating of the upper atmosphere. Journ. Geophys. Res. 70, 177

Jacchia, L. G. — 1965 — Static diffusion models of the upper atmosphere with empirical temperature profiles. Smithsonian Contrib. Astrophys. 8, 215-257

Jacchia, L. G. and J. Slowey — 1967 — The shape and location of the diurnal bulge in the upper atmosphere. Space Res. VII, 1077-1090

Johnson, F. S. — 1964 — Circulation at ionospheric levels. Report of the Southern Center of Advanced Studies, Contract CW-II, 19531

Kellog, W. W. — 1961 — Chemical heating above the polar mesopause in winter. Journ. Meteorol. 18, 373-381

Kellog, W. W.	1964	Pollution of the upper air by rockets Space Sci. Rev. 3, 275-316
King-Hele, D. G. and R. R. Allan	1966	The rotational speed of the upper atmosphere Space Sci. Rev., 6, 248-272
Kochanski, A.	1963	Circulation and temperatures at 70 - to 100 kilometer height Journ. Geophys. Res. 68, 213-226
Lindzen, R. S. D. Blake	1970	Mean heating of the thermosphere by tides Journ. Geophys. Res. 75, 6868-6871
Thomas, G. E. and B. K. Ching	1969	Upper atmospheric response to transient heating Journ. Geophys. Res. 74, 1796-1811
Volland, H.	1969	A theory of thermospheric dynamics-I Planet, Space Sci. 17,
Volland, H. and H. G. Mayr	1971a	A threedimensional model of thermospheric dynamics part I and II
Volland, H. and H. G. Mayr	1971b	The response of the thermospheric density to auroral heating during geomagnetic distirbances, to be published in Journ. Geophys. Res. 76,

Table I.

Coefficients in the series of spherical functions of pressure $\left(\delta^{f}_{n,n'}\right)$, latitudinal wind $\left(\psi^{f}_{n,n'-1}\right)$ and longitudinal wind $\left(\varphi^{f}_{n,n'}\right)$ for planetary wave modes with wave domain number n.

	pressure $\left(c_1\right)^{n_1}_{n} = \delta^{f}_{n,n'} \cdot \Delta_n$						latitudinal wind $\left(c_2\right)^{n_1}_{n} = \psi^{f}_{n,n'-1} \cdot \Delta_n$				longitudinal wind $\left(c_3\right)^{n_1}_{n} = \phi^{f}_{n,n'} \cdot \Delta_n$					
n \ n'	1	2	3	4	5	6	1	2	3	4	0	1	2	3	4	Δ_n
1	Δ_n	0	2/15	0	0	0	1	0	0	0	0	1	0	0	0	$1/5 - f_u f_v$
2	0	Δ_n	0	6/35	0	0	0	3	0	0	1	0	2	0	0	$3/7 - f_u f_v$
3	12/35	0	Δ_n	0	4/21	0	1	0	5	0	0	3	0	3	0	$7/15 - f_u f_v$
4	0	20/63	0	Δ_n	0	20/99	0	3	0	7	1	0	5	0	4	$37/77 - f_u f_v$

Table II

Relative pressure amplitudes p_n^f/p_o of the various planetary wave modes Θ_n^f deduced from the mesospheric winds observed at 92 km altitude. (f=0 : prevailing component ; f = f_1 : annual component ; f = f_2 : semiannual component)

n \ f	0	f_1	f_2
1	0	0.272	0
2	-0.082	0	0.005
3	0	-0.098	0
4	0.032	0	-0.081

FIGURE LIST

Figure 1. Mesospheric winds at 92 km height observed at Adelaide (35^{o} S) and Jodrell Bank (53^{o} N) versus time of year (solid lines) after Kochanski (1963) and theoretical winds (dashed lines).

Figure 1a. Meridional wind (N'ly = winds blowing from the north).

Figure 1b. Longitudinal winds (W'ly = winds blowing from the west).

Figure 2. Pressure function of the antisymmetric planetary wave mode $\theta_1^{\,0}$ versus co-latitude ϑ for five different heights within the thermosphere.

Figure 3a. Latitudinal wind function $\Psi_1^{\,0}$ and longitudinal wind function $\Phi_1^{\,0}$ versus co-latitude ϑ at 150 km altitude.

Figure 3b. Maximum wind amplitudes of the $\theta_1^{\,0}$ -mode versus altitude. (Solid line: positive; dashed lines: negative).

Figure 4. Pressure and wind functions of the antisymmetric planetary wave mode $\theta_3^{\,0}$ versus co-latitude.

Figure 5. Pressure and wind functions of the symmetric planetary wave mode $\theta_2^{\,0}$ versus co-latitude.

Figure 6. Pressure and wind functions of the symmetric planetary wave mode $\theta_4^{\,0}$ versus co-latitude.

Figure 7. Attenuation factors $\beta_n^{\,0}$ -1 ($\beta_n^{\,0}$ is the imaginary part of the eigenvalue of wave modes with wave domain number n.)

Figure 8. Relative wave amplitudes of pressure p and vertical wind w of the planetary wave modes versus altitude within the dissipative thermosphere ($z_o \sim 200$ km). The generating heat input is in phase with the pressure above the isobaric layer (solid lines) and is in antiphase with the pressure below that height (dashed lines). It terminates at z_o. Below that height, only downgoing free internal waves exist.

Figure 9. Meridional cross-section of the wind cell of the antisymmetric planetary wave modes with annual period f_1 during December-solstice. (Fig. 9a: $\theta_1^{f_1}$ -mode; fig. 9b: $\theta_3^{f_1}$ -mode.) Longitudinal winds are indicated by W = westerly and E = easterly.

Figure 10. Meridional cross-section of the wind cell of the symmetric planetary wave modes with semiannual period f_2 during equinox conditions. (Fig. 10a: $\theta_2^{f_2}$ -mode; fig. 10b: $\theta_4^{f_2}$ -mode.) Longitudinal winds are indicated by W = westerly and E = easterly.

Figure 11. Schematic picture indicating amplitude and phase relationship between the wind components near the turbopause and near the isobaric layer. Equator is on the left, poles are on the right. Longitudinal winds (E = winds from the east; W = winds from the west) in brackets yield for the southern hemisphere.

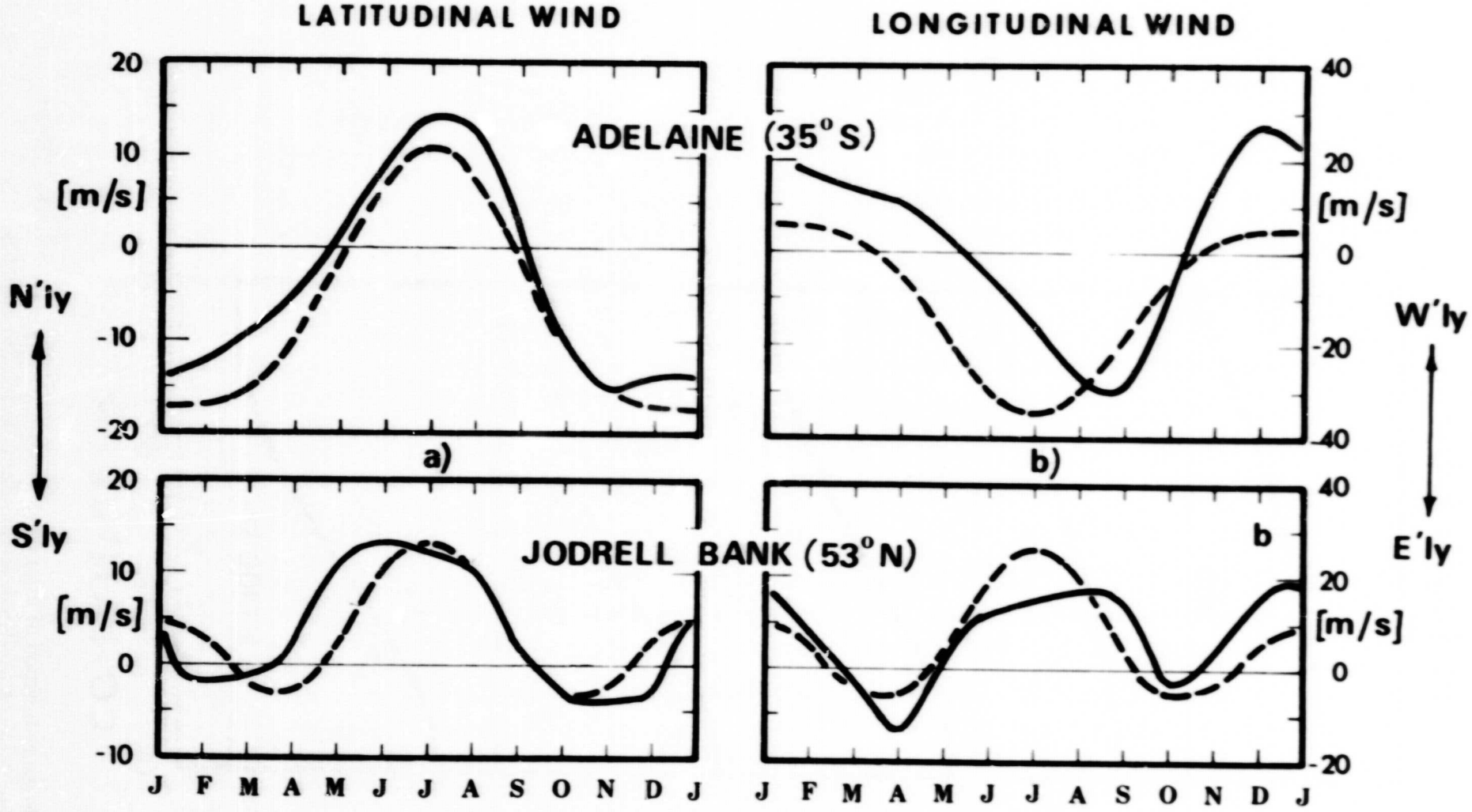

Figure 1. Mesospheric winds at 92 km height observed in Adelaine (35° S) and in Jodrell Bank (53° N) versus time of year (solid lines) after Kochanski (1963) and theoretical winds (dashed lines).

Figure 1a. Meridional wind (N'ly = winds blowing from the north).

Figure 1b. Longitudinal winds (W'ly = winds blowing from the west).

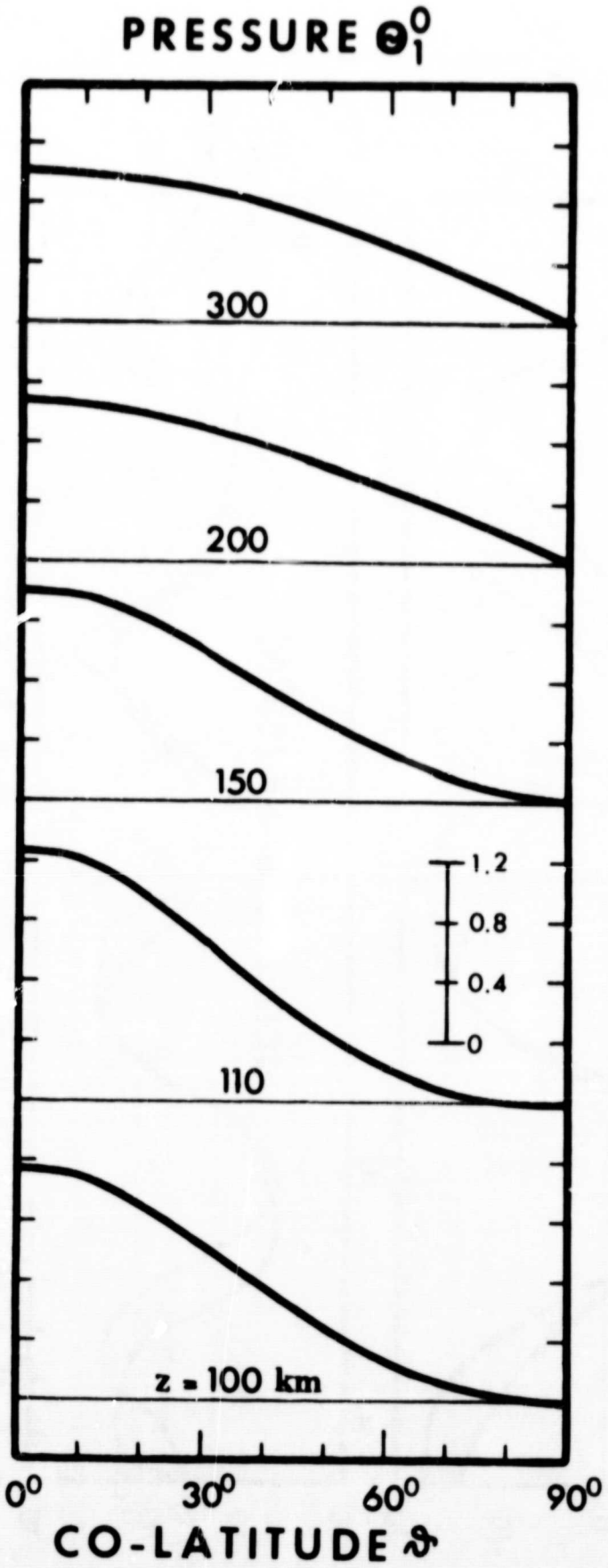

Figure 2. Pressure function of the antisymmetric planetary wave mode $\theta_1{}^0$ versus co-latitude ϑ for five different heights within the thermosphere.

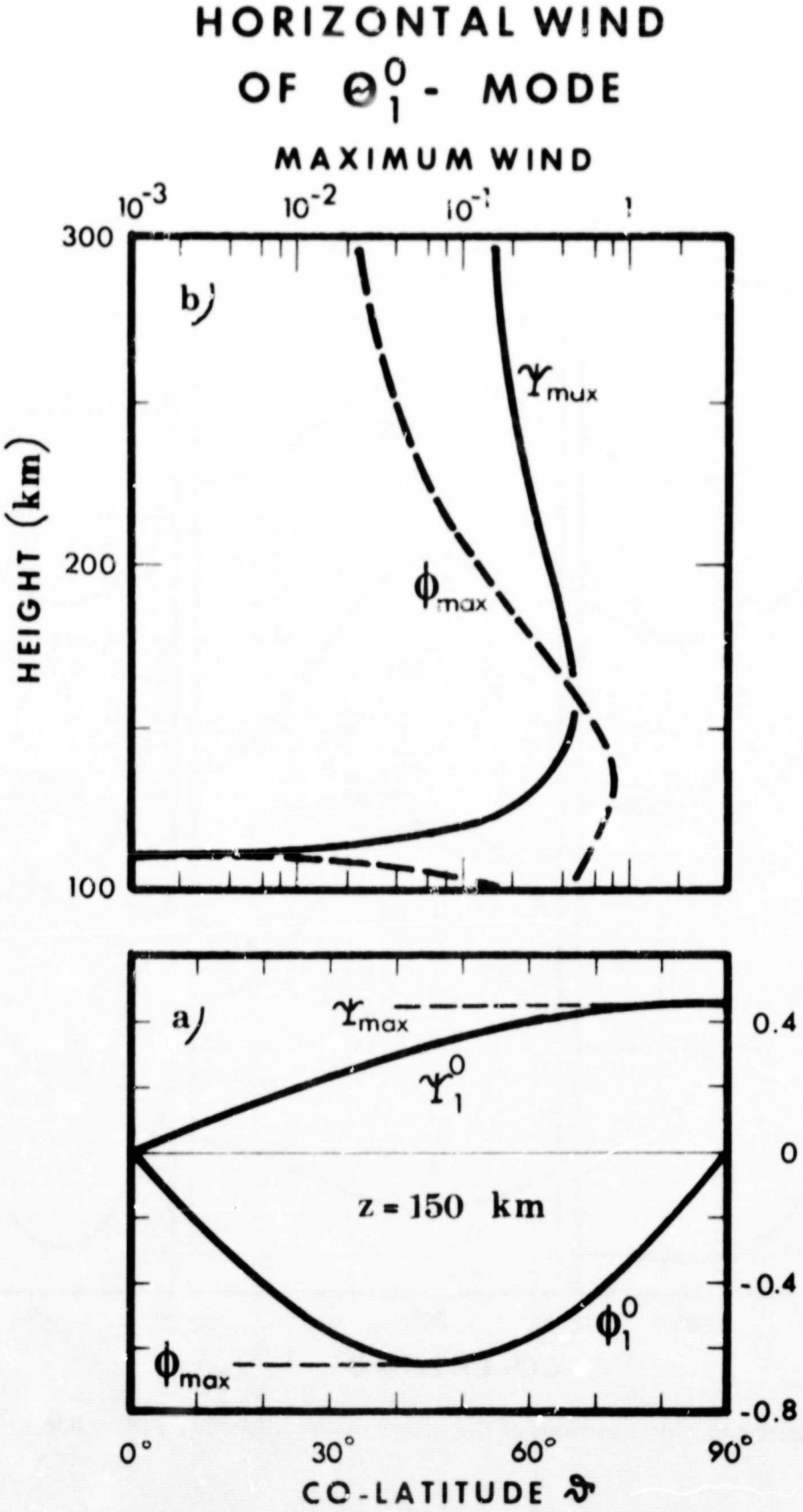

Figure 3a. Latitudinal wind function $\Psi_1{}^0$ and longitudinal wind function $\Phi_1{}^0$ versus co-latitude ϑ at 150 km altitude.

Figure 3b. Maximum wind amplitudes of the $\theta_1{}^0$ -mode versus altitude. (Solid line: positive; dashed lines: negative).

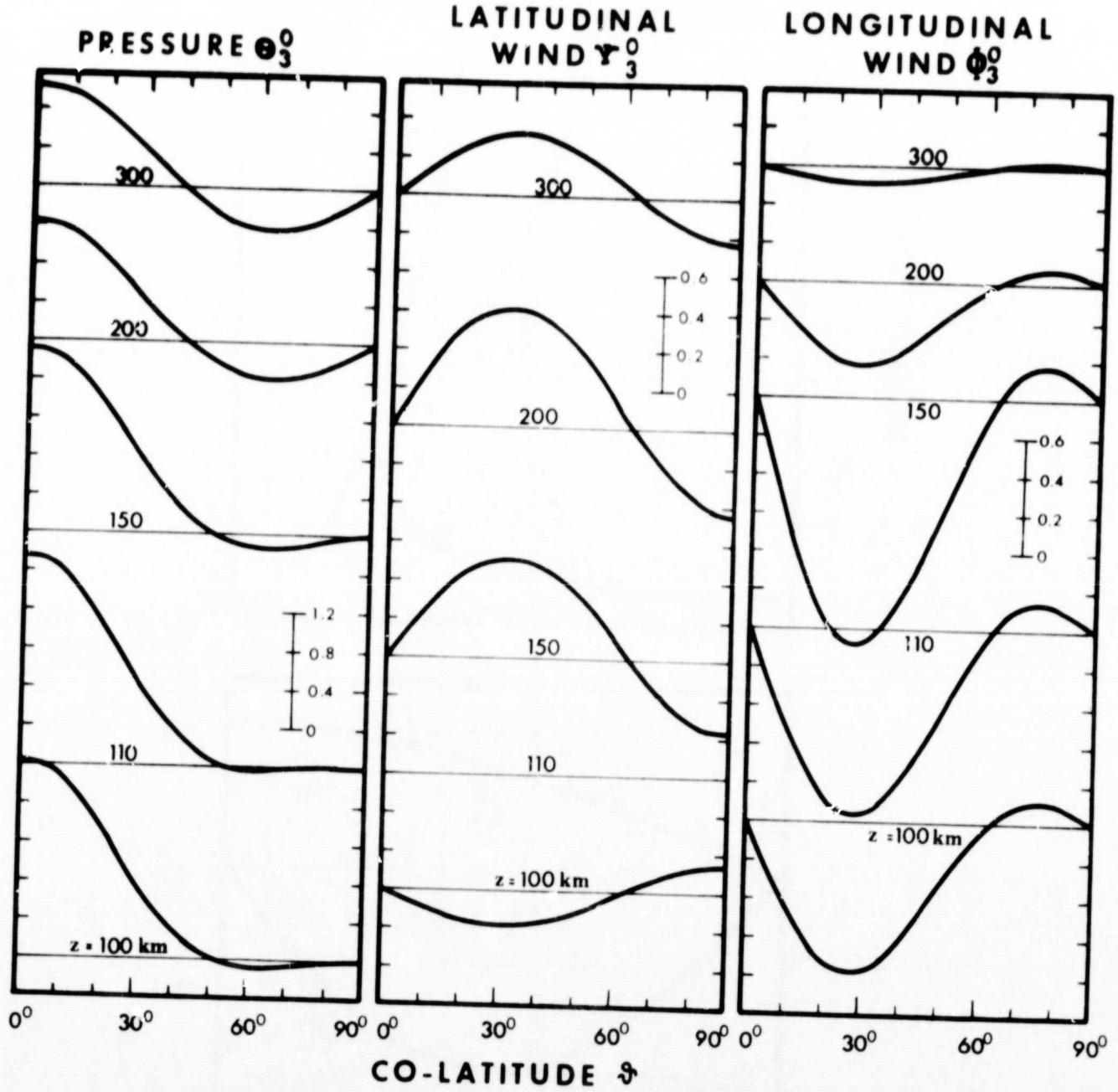

Figure 4. Pressure and wind functions of the antisymmetric planetary wave mode $\theta_3{}^0$ versus co-latitude.

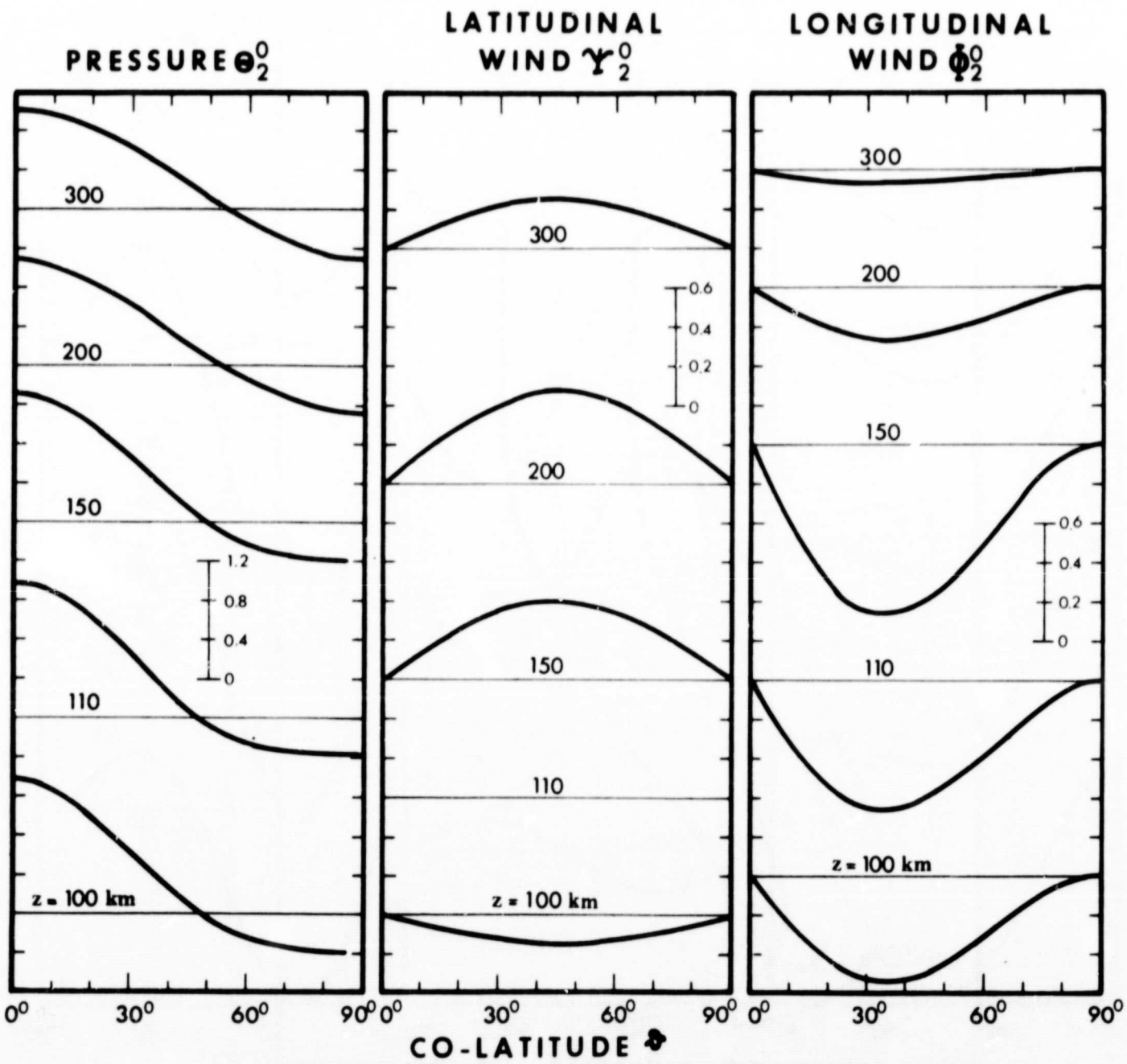

Figure 5. Pressure and wind functions of the symmetric planetary wave mode $\theta_2{}^0$ versus co-latitude.

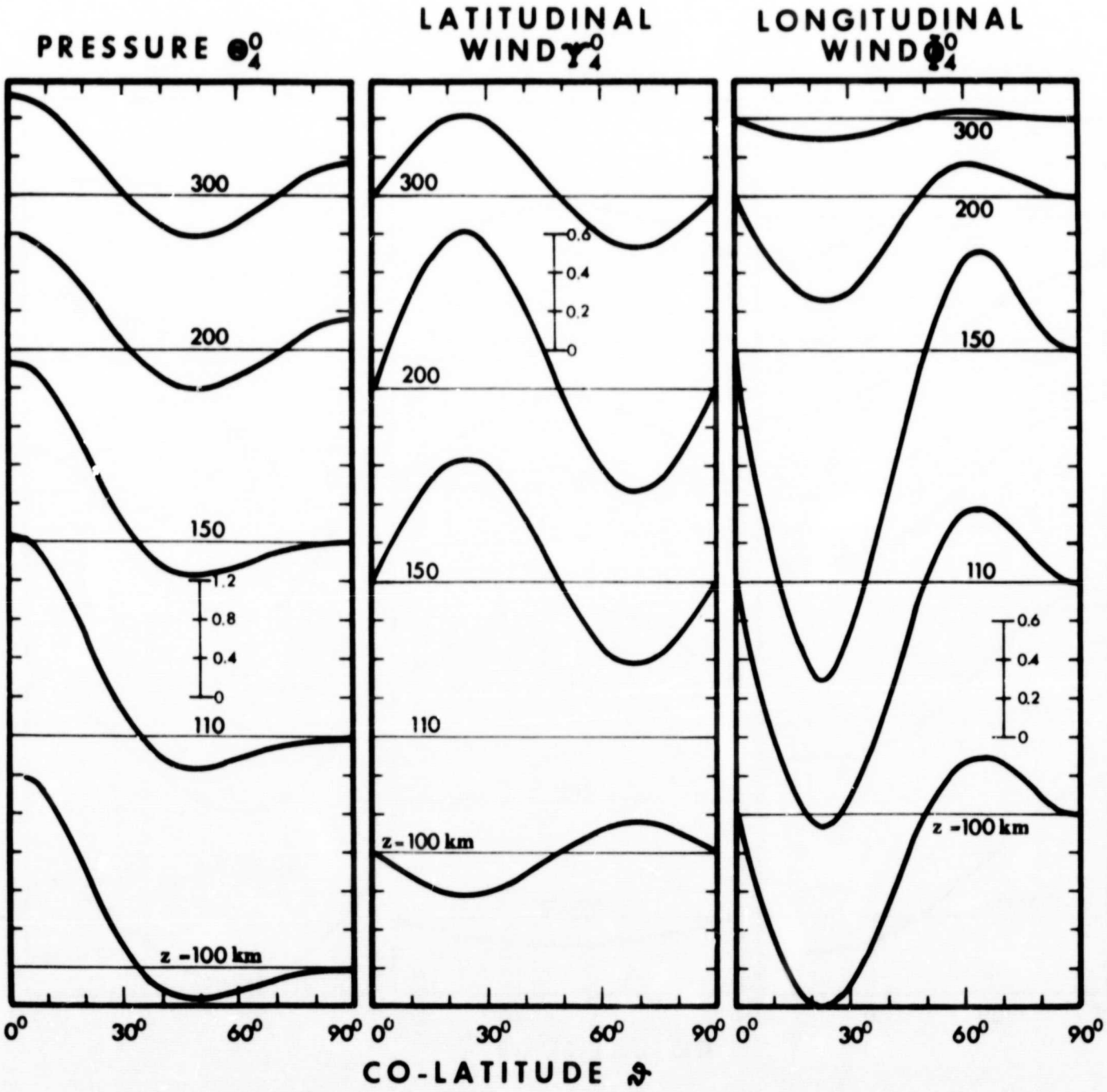

Figure 6. Pressure and wind functions of the symmetric planetary wave mode $\theta_4{}^0$ versus co-latitude.

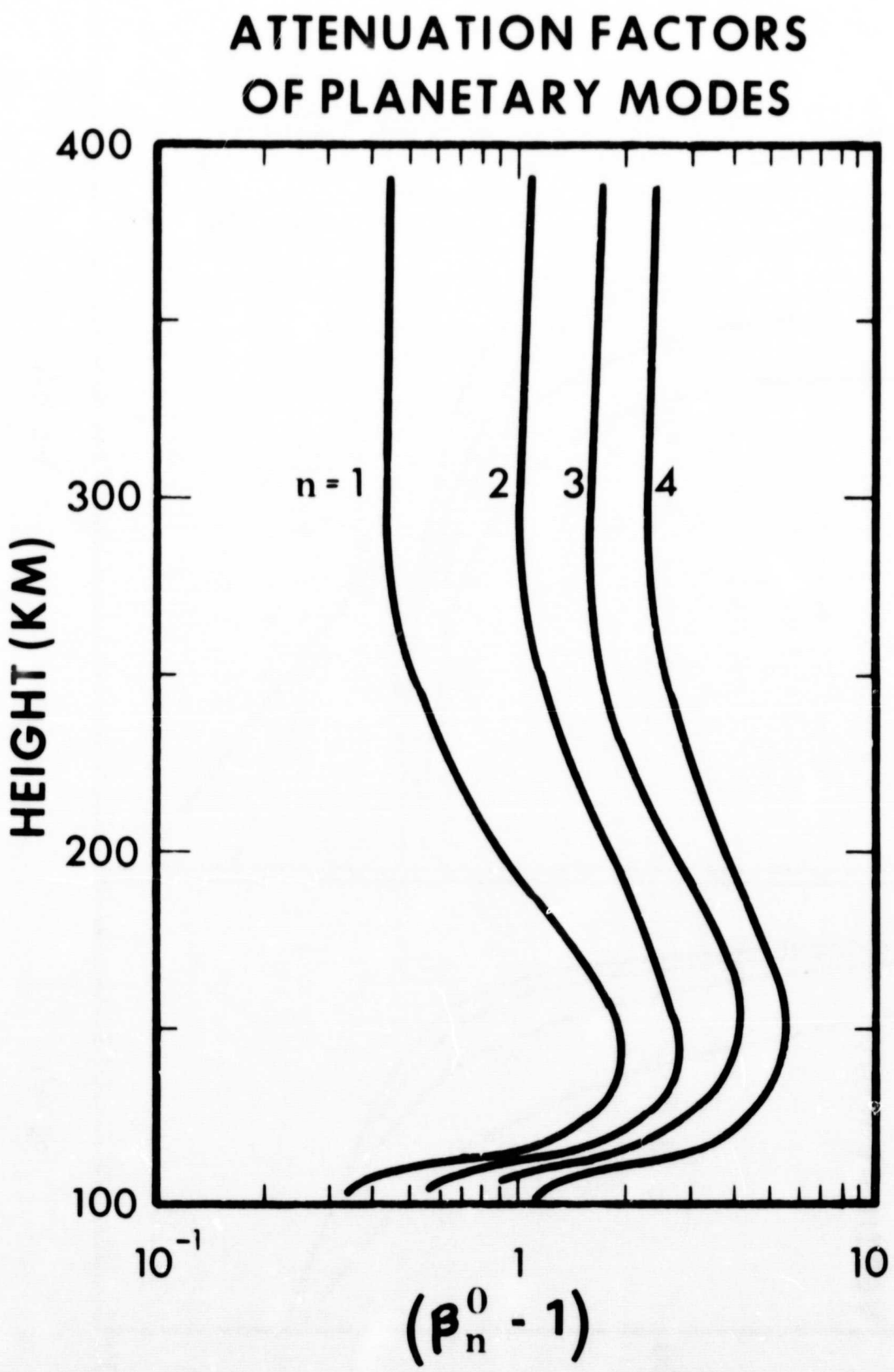

Figure 7. Attenuation factors $\beta_n{}^0$ -1 ($\beta_n{}^0$ is the imaginary part of the eigenvalue of wave modes with wave domain number n.)

WAVE AMPLITUDES OF PLANETARY MODES

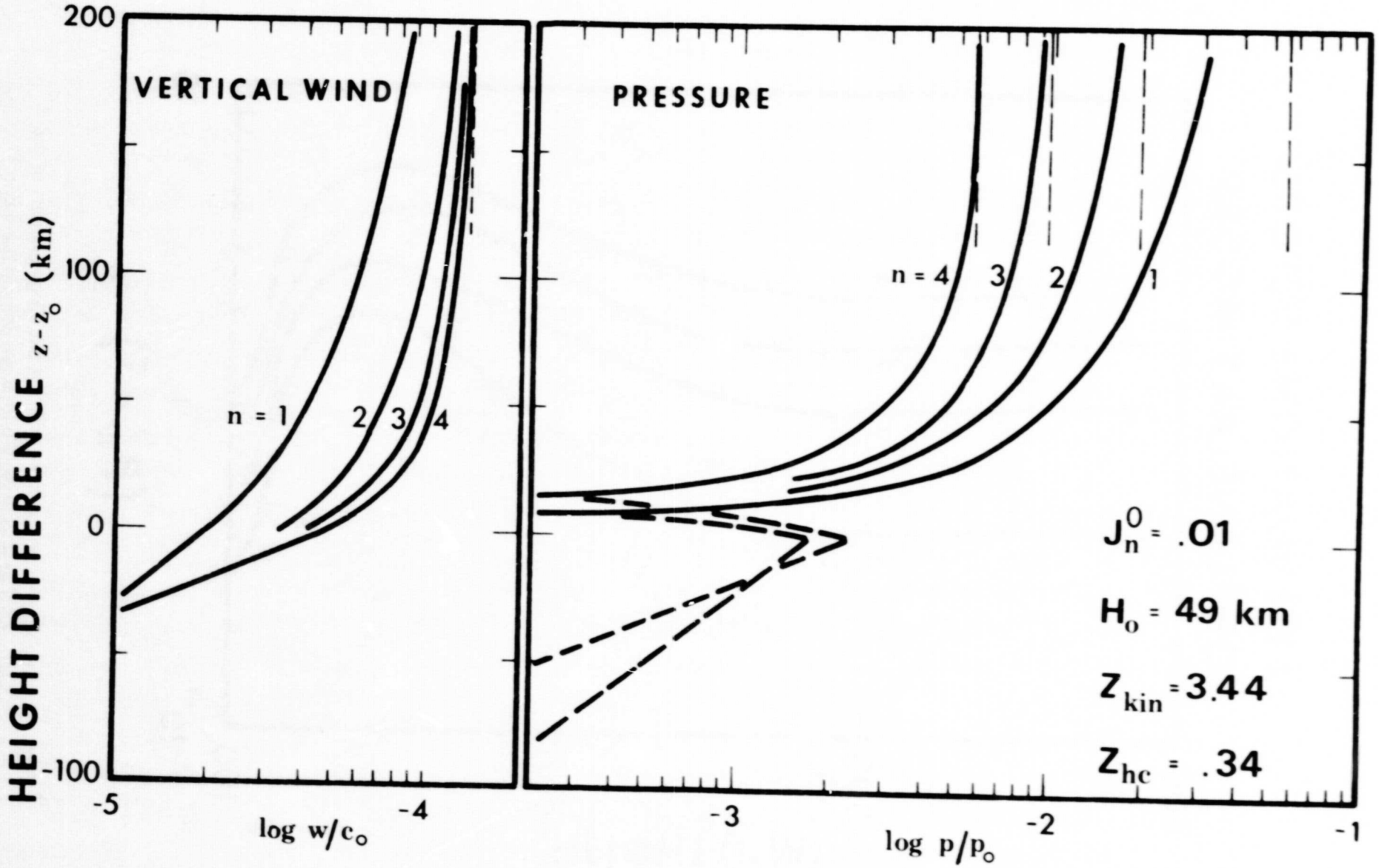

Figure 8. Relative wave amplitudes of pressure p and vertical wind w of the planetary wave modes versus altitude within the dissipative thermosphere ($z_o \sim 200$ km). The generating heat input is in phase with the pressure above the isobaric layer (solid lines) and is in antiphase with the pressure below that height (dashed lines). It terminates at z_o. Below that height, only downgoing free internal waves exist.

CIRCULATION CELLS OF SYMMETRIC PLANETARY MODES

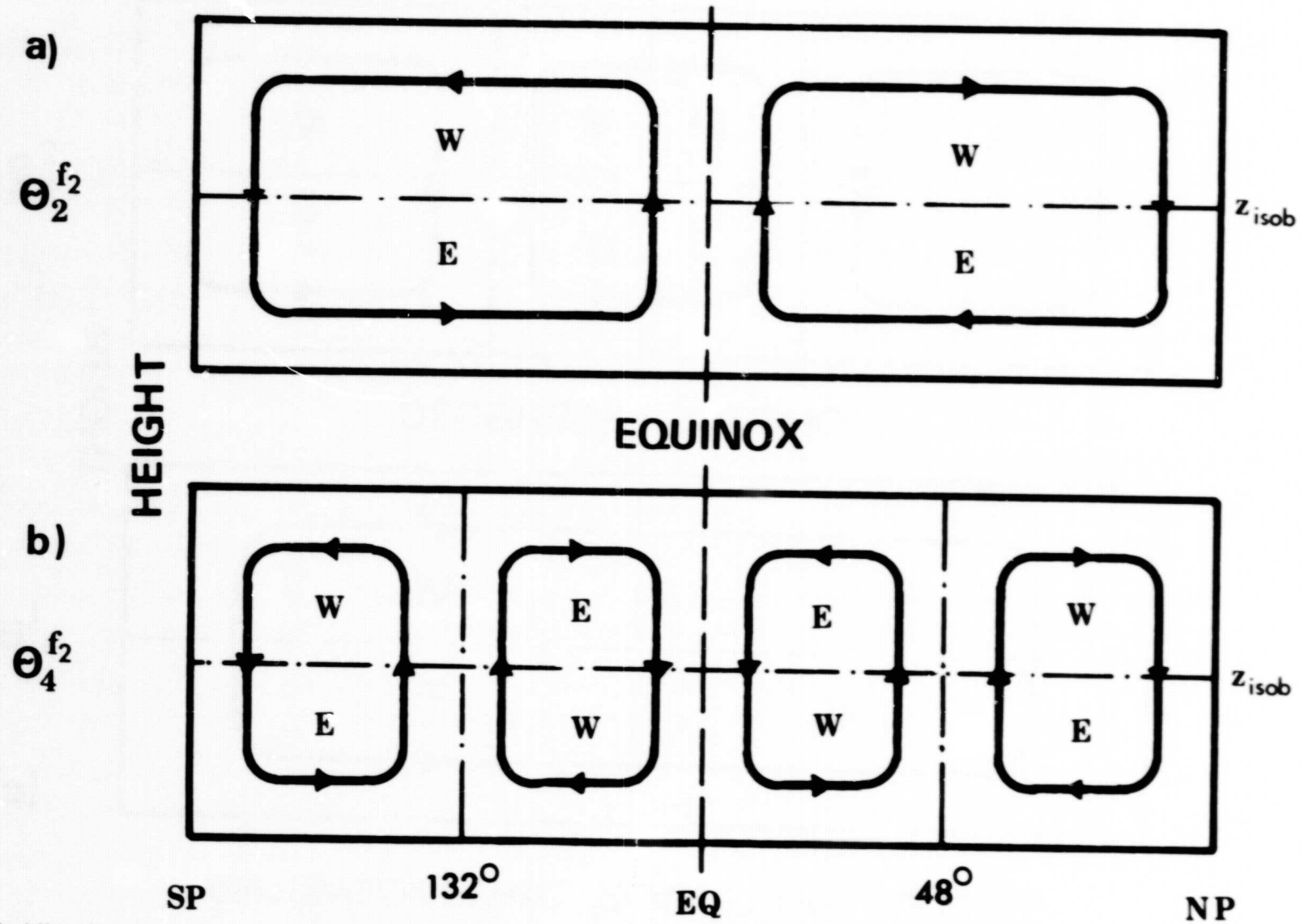

Figure 9. Meridional cross-section of the wind cell of the antisymmetric planetary wave modes with annual period f_1 during December-solstice. (Fig. 9a: $\theta_1^{f_1}$ -mode; fig. 9b: $\theta_3^{f_1}$ -mode.) Longitudinal winds are indicated by W = westerly and E = easterly.

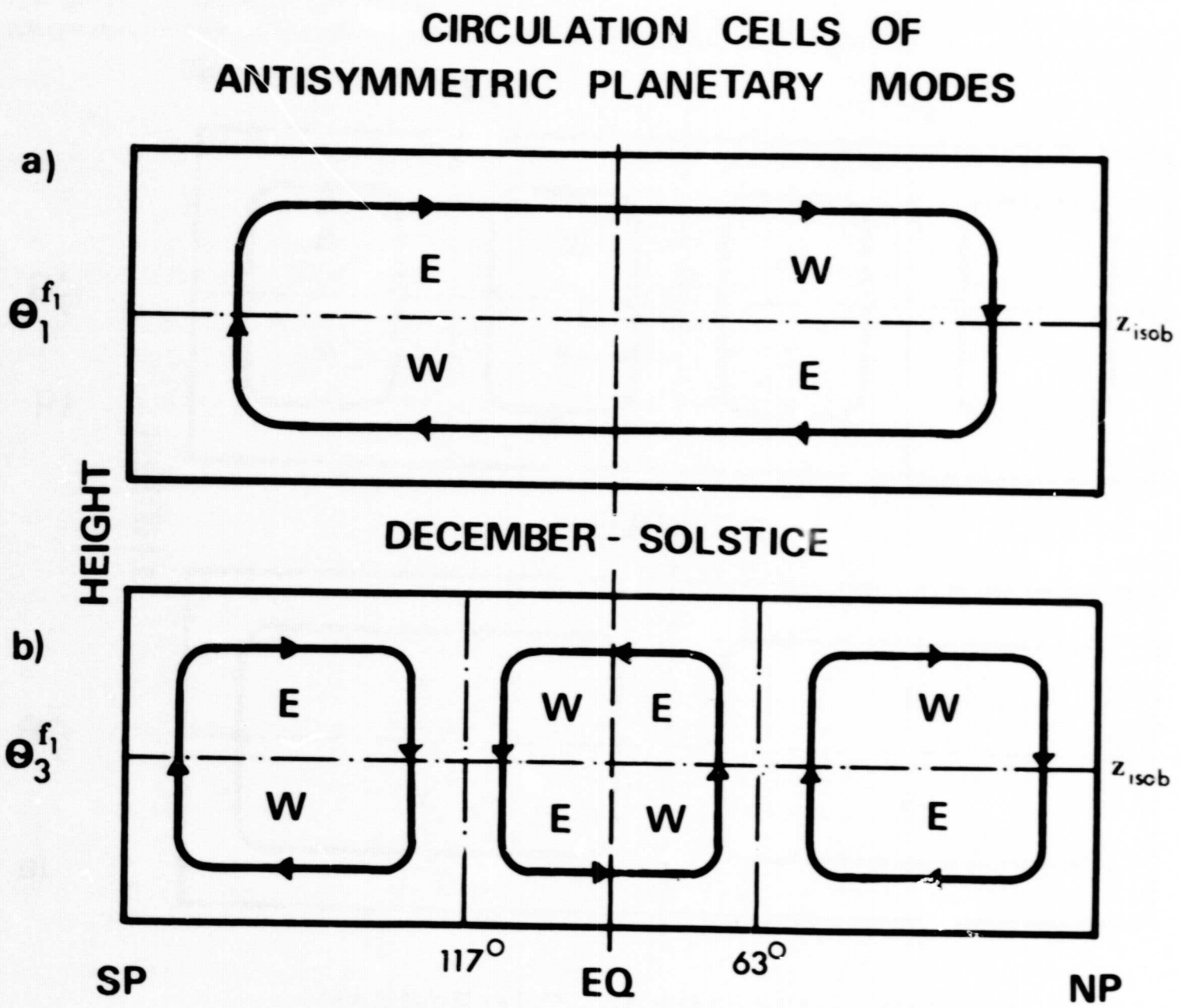

Figure 10. Meridional cross-section of the wind cell of the symmetric planetary wave modes with semiannual period f_2 during equinox conditions. (Fig. 10a: $\theta_2^{f_2}$ -mode; fig. 10b: $\theta_4^{f_2}$ -mode.) Longitudinal winds are indicated by W = westerly and E = easterly.

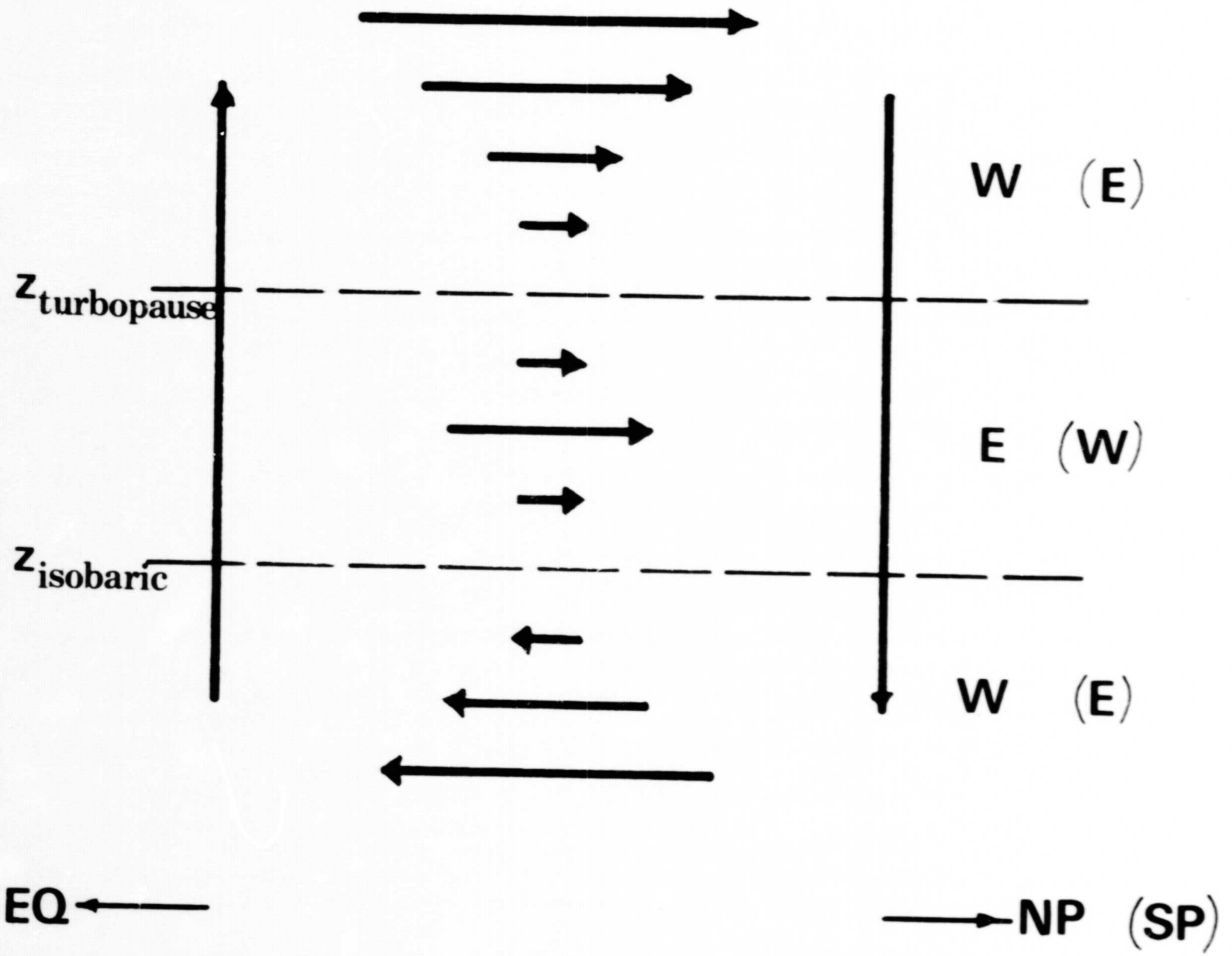

Figure 11. Schemiatic picture indicating amplitude and phase relationship between the wind components near the turbopause and near the isobaric layer. Equator is on the left, poles are on the right. Longitudinal winds (E = winds from the east; W = winds from the west) in brackets yeild for the = southern hemisphere.